TiO2 supported Co catalysts for the hydrogenation of γ-valerolactone to 2methyltetrahydrofuran: influence of the support

Emilia Soszka, Marcin Jędrzejczyk, Christophe Lefèvre, Dris Ihiawakrim, Nicolas Keller, Agnieszka Ruppert

TiO_2 supported Co catalysts for the hydrogenation of γ-valerolactone to 2-methyltetrahydrofuran: influence of the support

Emilia Soszka[a], Marcin Jędrzejczyk[a], Christophe Lefèvre[b], Dris Ihiawakrim[b], Nicolas Keller[c] and Agnieszka M. Ruppert*[a]

[a.] *Institute of General and Ecological Chemistry, Lodz University of Technology, ul. Żeromskiego 116, 90-924 Łódź, Poland. E-mail: agnieszka.ruppert@p.lodz.pl*

[b.] *Institut de Physique et Chimie des Matériaux de Strasbourg(IPCMS), CNRS/University of Strasbourg, 67034 Strasbourg, France.*

[c.] *Institut de Chimie et Procédés pour l'Energie, l'Environnement et la Santé (ICPEES), CNRS/University of Strasbourg, 67087 Strasbourg, France. E-mail: nkeller@unistra.fr.*

† Electronic Supplementary Information (ESI) available: XRD analysis, cell parameters of TiO_2 and Co phases, surface acidity analysis, H_2 uptake analysis in TPR, influence of the reduction temperature on the Co crystallite size, recycling results in the absence of pre-treatment, principle of the measurements of d-spacings from HRTEM images, additional catalytic data and FTIR spectra.

Abstract

2-Methyltetrahydrofuran (MTHF) is considered as one of the most promising green fuel alternatives that could be obtained from renewable lignocellulosic biomass through the catalytic hydrogenation of the γ-valerolactone (GVL) platform molecule. In the current work we report on the ability of earth-abundant non-noble metal Co catalysts supported on TiO_2 to be used efficiently for the synthesis of MTHF. The activity of TiO_2 supported Co catalysts in the hydrogenation of GVL to 2-MTHF was investigated, and several key factors with significant influence on the reaction have been identified and discussed. Among them we pointed out the crucial role of the titania support as a versatile tool able to drive the properties of the supported metallic cobalt nanoparticles and consequently the activity of the catalysts. In addition to the necessary catalyst acidity, we showed that the catalyst performances were related to the Co particle size and to the metal-support interaction, both properties being highly depending on the composition of the titania support. We demonstrated the beneficial co-presence of both anatase and rutile crystalline phases within the TiO_2 support, and we proposed that the crystalline phase nature is not only influencing the Co particle size and the catalyst acidity, but also allows to tune the SMSI effect for achieving optimum performances in 2-MTHF synthesis.

Introduction

The substitution of hazardous chemicals by more environmentally friendly alternatives and the production of sustainable chemicals and fuels from renewable resources has been recognized as one of the most promising current strategies for driving the

necessary environmental and energy transitions[1]. In this context, 2-methyltetrahydrofuran (2-MTHF) can be considered as ideal green alternative as it can be obtained from renewable sources such as lignocellulosic biomass. Indeed, 2-MTHF can be obtained through the hydrogenation of levulinic acid (LA) that is a hydrolysis product of lignocellulosic biomass. LA can be hydrogenated into γ-valerolactone (GVL), that can be further stepwise converted into 2-MTHF, first via the hydrogenolysis of the ester bond that yields to the 1,4-pentanediol (1,4-PDO) intermediate, and further via the subsequent dehydration of 1,4-PDO (Scheme 1). The production of 2-MTHF from GVL substrate is part of a complex reaction network with multiple (ring opening) hydrogenation and dehydration side steps that are competing with the straightforward two-step sequence of cyclic ester bond hydrogenolysis and subsequent cyclisation into 2-MTHF, and that are in consequence responsible for the formation of by-products crucial for the selectivity issues.

2-MTHF is considered as one of the promising biofuels or fuel additives competitive with ethanol or GVL, thanks to its high energy density and to its very low water solubility[2]. What is more, 2-MTHF can be used as a bio-derived solvent as due its low miscibility with water, excellent stability, and high boiling point. Additionally, preliminary toxicological tests suggest that 2-MTHF may be also used in pharmaceutical chemistry-related processes. Moreover, it should be emphasized that 2-MTHF can be abiotically degraded under air upon sunlight irradiation, possibly through oxidation and ring opening, which is in line with the principles of green chemistry[2,3].

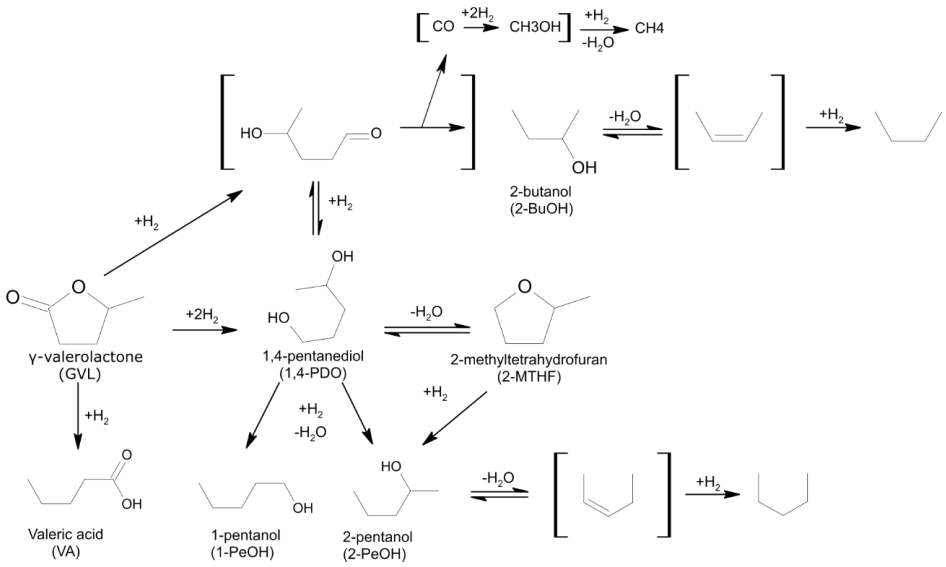

Scheme 1. Overall reaction pathways of the stepwise hydrodeoxygenation of GVL into 2-MTHF.

The initial hydrogenation of LA to GVL has been already successfully studied on many catalysts and is reported to occur with good yields over a broad range of reaction conditions. In the stepwise hydrodeoxygenation of GVL into 2-MTHF, the formation of the 1,4-PDO intermediate is often considered as the rate determining step[4]. The thermodynamics of the ring opening hydrogenation depends on the breaking of the C–O bond, and the cyclic ester hydrogenation involved in the conversion of GVL to 1,4-PDO which is endergonic with ΔG_0 = 70 kJ mol^{-1} at 250°C derived from thermodynamic calculations Severe reaction conditions such as high temperature and pressure are therefore usually required, although the exothermic nature of the hydrogenation reaction favors it at lower temperatures[5]. The 1,4-PDO intermediate must be further dehydrated to generate 2-MTHF, the dehydration reaction being considered as being close to thermoneutral (ΔH = -3 kJ mol^{-1}). The production of 2-MTHF requires in

consequence catalysts with well-balanced ring opening, hydrogenation and dehydration functions to target high selectivities and yields.

Among the noble metal-based systems, the Ru/C catalysts were broadly investigated. Al-Shaal et al.[6] studied the influence of the reaction temperature on the catalytic performance of a commercial 5%Ru/C catalyst. They observed that the hydrogenation of GVL was stimulated by high temperatures and pressure, and a complete GVL conversion was achieved in solvent-free conditions at 190°C and 100 bar of H_2 with a 43% yield to 2-MTHF within 24 h of reaction. They further highlighted the importance of the solvent, revealing that the presence of water in the reaction inhibits the dehydration step and favors the formation of 2-pentanol instead of 2-MTHF. Licurs et al [7] in their study with the combination of Ru/C, Re/C and niobium phosphate as acid co-catalysts showed that is possible to reach high selectivity towards 2-MTHF when high catalyst loading is used (nearly 64% selectivity with 38 % of GVL conversion was obtained at 200°C under 50 bar H_2 in 3 h of the reaction).

From a perspective of global resource sustainability and of lower environmental impact, there is now an intense focus on the use of cheaper, earth-abundant non-noble metals as catalysts for the formation of 2-MTHF, amplified further by a higher stability often reported. Sun et al.[8] demonstrated the influence of the calcination temperature on the catalytic performance of a commercial Cu/Al_2O_3 catalyst containing 55% CuO. They reported that a high calcination temperature (700°C) was necessary to achieve a high GVL conversion, ascribed to the relatively large size of Cu crystallites (30-60 nm) and to the presence of acid sites, while by contrast a too high calcination temperature such as 800°C favored the formation of the $CuAl_2O_4$ phase, which reduced the activity

of the catalyst. This very high Cu loading was however necessary to obtain a high selectivity to 2-MTHF with a nearly full conversion of GVL.

Obregon et al.[9] proposed that the formation of Ni-Cu alloy in Al_2O_3 supported bimetallic catalysts was responsible for the high activity observed, with a 64% yield to 2-MTHF being reached for 5 h of reaction conducted at 230° with 50 bar of H_2. Unfortunately, the catalyst suffered from redhibitory instability and no regenerative treatment allowed the catalyst to fully recover its initial activity. From another hand, Liu et al.[10] reported that the formation of a Cu-Zn alloy on the Al_2O_3 support promoted the synthesis of 1,4-PDO instead of 2-MTHF, as the highest selectivity to 2-MTHF (81%) was obtained with a monometallic Cu catalyst for a reaction performed in dioxane at 200°Cwith 40 bar H_2.

A very nice proof of principle study demonstrating the high activity of a Co-based catalyst supported on SiO_2 in the hydrogenation of LA to 2-MTHF was first reported by Novodárszki et al.[11] an appropriate selection of the reaction conditions in terms of temperature and H_2 pressure allowed the authors to implement a solvent-free LA hydrodeoxygenation process towards the selective production of 2-MTHF. They showed that the catalyst activity was strongly influenced by the reaction temperature. Indeed, the Co catalyst was active and stable in the hydrogenation of LA to GVL at 200°C, while increasing the temperature to 225°C increased the activity of the catalyst and resulted in high yields to 2-MTHF. The highest performance was obtained by using a Co loading of 8%, for which a 2-MTHF yield of 70% was achieved after 8 h of reaction at 225°C with 30 bar H_2 and maintained for 30 h.

Form the other hand, it is known that the properties of the support can strongly influence the performance of the catalysts. In particular, reducible titania supports are considered as a versatile tool given a driving force for modifying the properties of the supported metal nanoparticles and consequently the activity of the catalysts. For instance, in the case of the synthesis of lactone such as γ-butyrolactone or γ-valerolactone, Ru catalysts with different properties in terms of mean particle size, metal-support interaction strength or acidity were elaborated depending on the physico-chemical properties of the titania support, including notably its rutile or anatase crystallographic nature, with direct influence on the catalytic behavior[12]. In the case of the hydrogenation of succinic acid, the presence of the rutile polymorph phase in the TiO_2 support was proposed not only to favor the formation of small Ru particles, but also to promote stronger metal–support interaction compared to the anatase polymorph, both features being key factors driving the performances of the Ru/TiO_2 catalysts[13].

The direct influence of the TiO_2 support nature does not remain restricted to Ru-based catalysts. Indeed, for the same reaction, the group of Pinel showed that the nature of the TiO_2 support influenced the conversion obtained on Pd catalysts rather than the selectivity, the highest conversion being observed for anatase-supported samples and ascribed mainly to a good dispersion of the metal, while lower conversions were obtained using a mixed phase anatase/rutile TiO_2 support[14]. The catalytic performance of TiO_2 supported Ni catalysts in the HMF hydrodeoxygenation was also significantly impacted by the nature of the TiO_2 support. By influencing strongly the properties of the supported Ni nanoparticles, the reaction selectivity was tuned

towards specific products. Particularly, Ni catalysts supported on hydrothermally prepared TiO_2 exhibited relatively small surface acidity and large Ni particles, and allowed the 2,5-bishydroxymethyltetrahydrofuran biopolymer precursor to be selectively obtained. By contrast, the use of large surface area anatase as support stabilized small size Ni particles and the resulting Ni catalysts displayed a low surface acidity, what in turn orientated the reaction selectively towards the 2,5-dimethylfuran biofuel additive[15].

Therefore, the aim of the current work was to study the influence of the TiO_2 support nature on both the conversion and selectivity patterns in the hydrogenation of GVL to 2-MTHF over Co/TiO_2 catalysts. To this end, the potential of Co catalysts supported on different titania materials was investigated. We studied to which extent the 2-MTHF synthesis was influenced by the main physico-chemical properties of the Co/TiO_2 catalysts for deriving the key-factors responsible for the catalyst performances.

Experimental

Materials and Chemicals

$Co(NO_3)_2x6H_2O$ (99.9%, Eurochem, Poland) was used as received. Different TiO_2 materials were used as supports. Anatase-rutile mixed phase Aeroxide© TiO_2 P25 and P90 were delivered by Evonik-Degussa (Germany). MPT625 and ST01 consisting of pure rutile and anatase TiO_2, respectively, were delivered by ISK (Japan). CristalACTIV PC500 and G5 consisting of pure anatase TiO_2 were delivered by Cristal-Tronox. γ-Valerolactone (99%) was purchased from Sigma Aldrich.

Catalyst preparation

Catalysts with 10 wt.% of Co content were prepared through the wet impregnation method of different types of TiO_2 as supports using $Co(NO_3)_2x6H_2O$ as precursor of metal and water as solvent. After the solvent evaporation, all catalysts were dried at 120°C for 2h, calcined at 500°C for 5h under a flow of air with a heating rate of 5°C min^{-1}. The samples were further cooled down to room temperature and finally reduced under H_2 flow for 1h at a given temperature with a heating rate of about 25°C min^{-1}.

Characterization techniques

X-ray diffraction (XRD) measurements were performed on a PANalyticalX'Pert Pro MPD diffractometer using a Cu long-fine focus XRD tube working at 30 mA and 40 kV as X-ray source. Data were collected in the 5-90° 2θ range with a 0.0167° step and a 1 s integration time. The XRD patterns were investigated by Rietveld refinement with the Fullprof software for which the modified Thompson-Cox-Hasting function was chosen to generate the line shape of the diffraction peaks. Instrumental broadening has been previously determined by measuring the scattering from corundum (NIST standard SRM 1976b)[16, 17]. The mean crystallite size for TiO_2 and Co phases defined as the average size of the coherent diffracting domains, was derived from the whole XRD patterns after refinement and determined from the Scherrer equation with the usual assumption of spherical crystallites taking into account the intrinsic broadening of the peaks due to the instrumentation.

Temperature-programmed reduction (TPR) was performed on AMI1 system from Altamira Instruments, USA, using a thermal conductivity detector for studying the catalyst reducibility. Before the measurement, the calcined catalysts were heated up

to 300°C (with a 10°C/min heating rate) to remove of impurities from the sample surface for 30 min, using a mixture of 2 vol.% O_2 and 98 vol.% Ar. The TPR profiles were recorded from 35°C up to 800°C, with a temperature ramp of 10°C min^{-1}, using a mixture of 5 vol.% H_2 and 95 vol.% Ar at a space velocity of 3.1 x 10^{-9} g s^{-1} cm^{-3}.

Temperature-programmed desorption (TPD) of NH_3 was used to study the acidity of the catalysts. The NH_3-TPD experiments were implemented in a home-made quartz-based flow micro-reactor. Before all experiments, the freshly reduced catalysts surface was purified under a flow of He at 500°C for 30 min. The catalyst was then cooled down to 100°C, and NH_3 was adsorbed on the surface of the catalyst for 15 min at 100°C. Before TPD-NH_3 measurement, physically adsorbed NH_3 has been removed from the catalyst surface by purifying the sample with He carrier gas for 15 min and then cooled to room temperature. The NH_3-TPD experiment was performed from room temperature to 500°C with a 25°C min^{-1} heating ramp.

Co/TiO_2 on different supports	**Crystalized phase composition [%]**		**Average crystallite size of R and A [nm]**	**Average crystallite size of Co [nm]**	**BET surface area [m^2/g]**	**Acidity [µmol/m^2] ([µmol/g])**
	R	**A**				
Rut	100	0	9(1)	11	68	4.1 (279)
P25	20	80	A:18(1) ; R:26(1)	4	49	6.5 (316)

P90	10	90	A:12(1) ; R:10(1)	6	65	3.3 (217)
G5	0	100	11(1)	11	88	4.1 (358)
PC500	0	100	12(1)	11	89	3.7 (329)
ST01	0	100	13(1)	6	89	2.5 (224)

Table 1. The main physico-chemical properties of the 10%Co/TiO_2 (red. 500°C) catalysts.

Fourier Transform InfraRed spectra (FTIR) of adsorbed CO were recorded on a Nicolet 6700 spectrometer equipped with a liquid nitrogen cooled MCT detector and a diffuse reflectance environmental chamber. The catalyst reduced (at 500°C or 300°C) was placed in a sample holder, and re-reduced in situ at the same temperature in flowing 5% H_2/Ar for 1h, and cooled to room temperature under Ar flow before the background spectrum was recorded. CO adsorption was carried out at 3 bar pressure of 5% CO in Ar for 30 min. All spectra were recorded with a resolution of 4 cm^{-1} performing 64 scans. Spectra of post reaction titania were obtained by a transmission measurement using KBr technique with a ratio 1:100 sample to KBr.

Transmission electron microscopy (TEM) was performed using a JEOL 2100F microscope with a point resolution of 0.2 nm and operating at a 200 kV acceleration voltage. The samples were firstly grinded and sonicated in an ethanol solution, before a drop of the solution was deposited onto a copper grid covered by a holey carbon membrane for observation. The identification of the Co phases required the implementation of a suited HRTEM image processing applied to individual Co-based nanoparticles (see SI2), due to the similarity between certain planes of TiO_2 and of the Co phases.

Stability of the catalysts during the reaction was evaluated by inductively coupled plasma atomic emission spectroscopy (ICP-AES). Whatever the Co/TiO_2 catalyst, no Co leaching was observed during the reaction, as ICP analysis did not reveal the presence of Co traces in the post-reaction mixture.

Catalytic tests

The catalysts were tested in the γ-valerolactone (GVL) hydrogenation in high pressure reaction conditions. The activity tests were performed in liquid phase using 1,4-dioxane as solvent within a 100 mL stainless-steel reactor (Parr, Germany). The reactions were carried out with 1 g of GVL, 0.6 g of catalyst and 30 mL of 1,4-dioxane. The reactor was flush with hydrogen to remove air and the reactor was pressurized with hydrogen to 50 bar and the reaction was performed at 230°C for 5h with a stirring rate of 800 rpm[9,10,18]. The reaction conditions were selected for obtaining conversion levels allowing for a valid comparison of the catalyst performances, in agreement with the literature. The reactor was further cooled down and the pressure was released. The obtained reaction mixture was centrifuged to separate the catalyst from the solution. The liquid products were analyzed using an external standard on an Agilent 7820A GC instrument equipped with a CP-Wax 52 CB capillary column and a flame ionization detector.

GVL elimination, GVL conversion and product yields were calculated as follows:

$$Elimination\ (GVL) = \frac{n_{GVLi} - n_{GVLr}}{n_{GVLi}} \times 100\%$$

$$Yield\ (prod) = \frac{n_{prod}}{n_{GVLi}} \times 100\%$$

$$Conversion\ (GVL) = \frac{\sum n_{prod}}{n_{GVLi}} \times 100\%$$

n_{GVLi} and n_{GVLr} being the number of moles of GVL molecules before and after the reaction, respectively, and n_{prod} being the number of moles of a given product in the reaction mixture.

Results

Characterization of the 10% Co/TiO_2 catalysts

The physico-chemical properties of the 10% Co/TiO_2 catalysts after final reduction at 500°C are summarized in Table 1, and the XRD patterns of the catalysts are shown in Figure S1 with their corresponding profile Rietveld refinements.

The catalysts exhibit different phase compositions of the TiO_2 supports, namely pure rutile (Rut), mixed anatase/rutile phases (P25 and P90) and pure anatase phase (G5, ST01 and PC500), with reflexes indexed in the I41/amd and P42/mnm tetragonal unit cells of anatase and rutile TiO_2, respectively. They differ also in terms of specific surface area and of the associated mean TiO_2 crystallize size. Independently of the support phase composition, the specific surface area of the catalysts is directly related to the mean size of the TiO_2 crystallites, as it is ranging from 49 m^2/g for TiO_2 P25 to about 90 m^2/g for TiO_2 G5, PC500 and ST01, without any microporosity, and relates inversely to the mean crystallite size of the support ranged from 9 nm to 26 nm. In addition to the diffraction peaks assigned to both anatase and rutile phases of the TiO_2 support, the patterns show reflexes indexed in the Fm-3m cubic unit cell of metallic Co phase (JCPDS

Card No. 15–0806)[19]. The mean size of the metallic Co nanoparticles has been derived from the refinement starting from 4 nm (P25), 6 nm (P90, ST01) reaching 11nm (G5, PC500, Rut). It must be said that performing structural refinement was necessary, as the main diffraction peak of the metallic Co at 2θ=44.35° that corresponds to (111) crystal plane is partially overlapping with a secondary reflex of the rutile TiO_2 phase at 2θ=44.0° assigned to the (210) plane. The crystallographic data associated to the refined samples are provided in Table S1.

The acidity of the Co/TiO_2 catalysts was measured using NH_3 as molecular probe and reported In Table 1 (Figure S2). It was ranging from 216 µmol/g to 358 µmol/g, for the Co catalysts supported on P90 and G5, respectively. After normalization of the acidity values per surface area unit of the catalysts, to consider the surface nature of the acidity property, the surface acidity was within the 2.5-6.5 µmol/m^2 range, the lowest and highest values being obtained for the Co/ST01 and Co/P25 catalysts, respectively. The data indicated that the surface acidity of the catalysts has probably a multi-factorial origin, comprising notably the metal-support interaction as well as both Co nanoparticle and titania crystallite sizes. Indeed, no straight forward relationship with the main physico-chemical properties of the catalysts was found. For instance, samples with a similar Co nanoparticle size exhibited different surface acidities (P90, ST01), while similar surface acidities were obtained for catalysts based on pure anatase (G5) and rutile (Rut) supports. Figure S3 shows that, to some extent, specific relationships can be only partially drawn. Globally the surface acidity decreases with increasing the titania mean size whether it is composed of anatase or rutile phases (Fig. S3-D) and increases with increasing the Co/TiO_2 size ratio (Fig. S3-B), although the Co/P25 catalyst

with mixed anatase/rutile phase exhibits a totally different behavior in regards of both parameters. Also the rutile phase content in the TiO_2 support does not seem to be a key-parameter for the surface acidity of catalysts (Fig. S3-A), while the surface acidity was reported to decrease with increasing the titania anatase mean size for pure anatase-based catalysts (Fig. S3-C).

Temperature programmed reduction measurements. The reduction profiles of Co/TiO_2 catalysts are shown in Figure 1A, H_2 uptake being shown in Table S2. Independently of the catalyst, they were characterized by a broad multi-contribution envelope, with a two-step reduction of cobalt oxide to metallic cobalt being observed over a wide temperature range (280-600°C). The low temperature peak can be assigned to the reduction of Co_3O_4 to CoO, while the high temperature peak corresponds to the subsequent reduction of CoO to metallic cobalt [20,21,22]. The anatase supported samples displayed similar reduction temperatures, at ca. 325°C and 430°C. The presence of rutile in the TiO_2 support shifted both reduction peak maximum towards higher temperatures, so that temperatures higher than 550°C were required for achieving complete reduction into metallic Co on rutile-containing and pure rutile supports. The influence of the rutile phase content in the TiO_2 support on the temperature of complete reduction is depicted in Figure 1B, the maximum temperature of complete reduction of the supported phase is increasing with the increase in the rutile phase content in the support. Differences in the temperature of both reduction peaks and its complex shape might suggest the existence of different interactions between the TiO_2 surface and the supported Co phase[20,23]. The higher reduction temperature suggested that the Co nanoparticles exhibited stronger interaction with the rutile polymorph in comparison to the anatase counterpart.

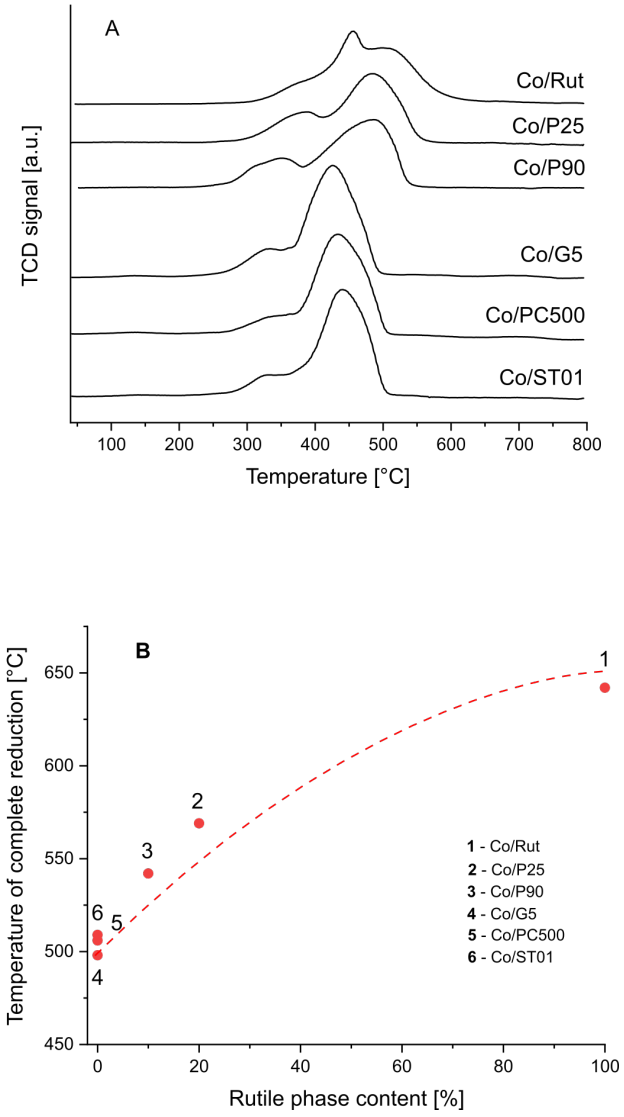

Figure 1. (A) TPR profiles of the Co/TiO_2 catalysts after the oxidation step at 500°C, and **(B)** influence of the rutile phase content in the TiO_2 support on the temperature of complete reduction.

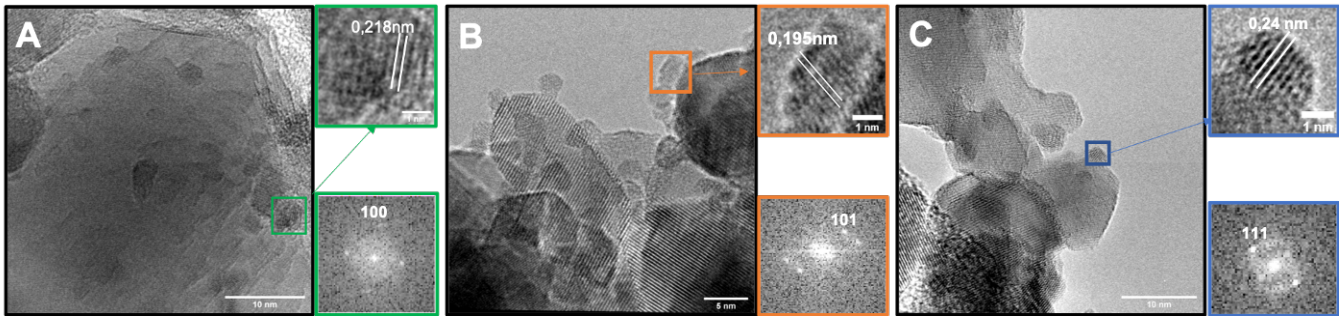

Figure 2. TEM and HRTEM images for (**A**) Co/P25-500, (**B**) Co/ST01-500 and (**C**) Co/ST01-300 catalysts for the identification of the nature of the Co phase. The top-right frames represent the HRTEM images recorded on an individual Co or CoO nanoparticle. The bottom-right frames correspond to the 2D fast Fourier transform (FFT) of the same framed nanoparticle.

Table 2. Catalytic efficiency of the Co/TiO_2 catalysts (red. 500°C) in the GVL hydrogenation in terms of yields to the different products, GVL elimination, GVL conversion and carbon imbalance.

Catalyst	Product yield [%]						GVL elimination [%]	GVL conversion [%] [a]	Carbon imbalance [%] [b]
	2-MTHF	BuOH	2-PeOH	1-PeOH	VA	PDO			
Co/Rut	33	0	1	3	2	3	86	42	44
Co/P25	76	0	5	0	0	0	97	81	16
Co/P90	43	4	1	5	0	3	89	56	33

Co/G5	3	0	1	0	4	0	30	8	22
Co/PC500	4	0	1	0	3	2	21	10	11
Co/ST01	8	0	0	0	3	2	46	13	33

Reaction conditions: 230°C; 5h; 0.6 g of catalyst, 1 g GVL; 30 ml 1,4-dioxane and 50 bar H_2

[a] the GVL conversion expressed as the sum of the different yields

[b] calculated as the difference between the GVL elimination and the sum of the different yields

The reduction of the supported phase is thus directly influenced by the composition of the TiO_2 support itself, and in consequence the force of the interaction with the support. This was in agreement with earlier results obtained on Ru/TiO_2 systems. Our previous works suggested that the rutile phase promotes stronger metal-support interaction compared to the anatase polymorph[13]. Further, the Weckhuysen's group reported that Ru nanoparticles were subjected to sintering on pure anatase supports, in contrary to what was observed in the case of pure rutile or rutile-containing supports[24], and in agreement with the works of the Crossley's group, that evidenced that rutile support prevents from the sintering of supported Ru nanoparticles[25]. Interestingly the ability of RuO_2 phase to migrate from the anatase to the rutile phase in polymorphic TiO_2 supports was also proposed by Kim et al. to suggest stronger interactions between the rutile phase and the supported Ru phases[26].

Transmission electron microscopy. HRTEM characterization of the Co/TiO_2 catalysts demonstrated the high crystallinity of the cobalt nanoparticles supported on TiO_2, the inter-planar spacings between atomic plans being identified. Regardless of the TiO_2 nature, the samples reduced at 500°C confirmed the presence of metallic Co, as exemplified in Figure 2A-B in the case of both Co/P25 and Co/ST01 catalysts, for which inter-plane distances of 0.218 nm and 0.195 nm characteristic of the (100) and (101)

planes of hexagonal metallic Co, respectively, were observed through the application of a suited image processing (Figure S4).

Catalytic activity

Table 2 shows the performances of the Co/TiO_2 catalysts in the hydrogenation of GVL. Catalysts supported on different titania varying in terms of phase composition, average crystallite size and specific surface areas were studied. Whatever the Co/TiO_2 catalysts, 2-MTHF was the main reaction product. The highest yield to 2-MTHF was achieved using the mixed anatase/rutile TiO_2 P25 as support, namely 76%, with residual yield to 2-PeOH side product of 5%. The Co/P25 catalyst strongly outperformed its counterparts based on the anatase/rutile mixed phase (P90) and pure rutile (Rut) supports, that allowed for 2-MTHF yields of 43% and 33%, respectively, with also in both cases very low yields to side products. By contrast, only very low yields to 2-MTHF (lower than 10%) were obtained on the catalysts based on the pure anatase phase support (G5, PC500, ST01), the lowest yield of 3% being obtained on the Co/G5 catalyst.

A carbon imbalance was observed whatever the catalyst tested, as the sum of yields was not matching with the observed deficit in the GVL substrate (non-closure of the carbon balance). Indeed, the sum of the different product yields remained lower than the level of GVL elimination, with mismatch values ranging from 11% to 44% depending on the catalyst. Among the most active catalysts, the higher carbon imbalance was observed for the Co/Ru catalyst, *ie.* 42% *vs.* 86%, while the lowest mismatch was obtained for the Co/P25 catalyst giving the highest 2-MTHF yield, namely 81% *vs.* 97%.

Considering the affinity of acids such as the valeric acid (VA) reaction product with the surface hydroxyl groups of the TiO_2 support, the surface of the tested catalysts was

washed with dioxane solvent. The HPLC analysis of the resulting mixture confirmed that the carbon imbalance observed did not result from the storage of VA or of other surface intermediates bound to the TiO_2 surface during the catalytic test. By contrast, traces of the GVL reactant were detected.

A series of complementary tests shown in Table S3 were in consequence conducted by submitting the GVL substrate and the TiO_2 support alone to the reaction conditions for 5h. While no significant decrease in GVL was observed in the absence of TiO_2, a strong reduction in the GVL content within the 30-39% range was obtained in the presence of the support alone in the case of P25, P90 and ST01. However, this GVL elimination was not concomitant with the formation of 2-MTHF or with any other reaction products, independently of the TiO_2 support used. A similar result was obtained when the P25 support was reduced at 500°C prior to the test. FTIR analysis spectra shown in Figure S5 revealed further an increase in the intensity of the band associated with the carbonyl group when the P25 support was submitted to the reaction conditions in the presence of GVL. This confirmed the strong interaction of the GVL substrate with the TiO_2 support. This was in line with the findings of Huang et al. who concluded that the adsorption of the GVL substrate in the presence of a nonpolar hydrocarbon-type solvent occurred mainly on the oxide support rather than on the metal sites in the case of a Ni-Cu/Al_2O_3 catalyst[27]. They showed further that 2-MTHF was less prone to adsorb than GVL due to their polarities and structural differences, in agreement with DFT calculations (Table S3). They proposed that the stabilization of the hydrogen bond interaction between the hydroxyl H atom of the Al_2O_3 surface and the carbon oxygen atom of GVL contributes to the highest adsorption energy of GVL. This

correlates well with the result of the control experiment consisting in submitting the 2-MTHF substrate to the reaction conditions in the presence of the pure TiO_2 support, for which no decrease in 2-MTHF was observed (Table S3). On a Co/SiO_2 catalyst, Novodárszki et al. proposed that GVL is mainly adsorbed on the weak acid silanol groups of the silica support *via* its ring O-atom and/or the carbonyl group, as supported by Quantum chemical calculations and DRIFT spectroscopic results[28].

The carbon imbalance observed independently of the Co/TiO_2 catalyst tested was therefore proposed to result from the adsorption of non-reacted GVL substrate at the catalyst surface. This was confirmed by the increase in the 2-MTHF yield and the strong reduction of the carbon imbalance observed when prolonging the reaction time from 5 h to 6 h on the Co/P90 catalyst, what favours the further conversion of adsorbed (non-reacted) GVL into 2-MTHF, while keeping the same GVL elimination (Table S4). This highlights that the decrease in GVL observed in the reaction conditions cannot be ascribed fully to the GVL conversion as it comprises also the GVL remaining adsorbed at the catalyst surface, so that the term GVL elimination was here preferred. Therefore, the GVL conversion can be preferably expressed as the sum of the yields to the different products. 2-MTHF being the major product observed, the catalysts followed the same ranking order in terms of GVL conversion *vs.* 2-MTHF yield. Indeed, the Co/P25 catalyst outperformed both Co/P90 and Co/Rut catalysts, with conversion of 81% *vs.* 56% and 42%, respectively. On another hand, very low GVL conversions were obtained on the catalysts based on a pure anatase TiO_2 support, *ie.* 13%, 10% and 8% for the catalysts supported on ST01, PC500 and G5, respectively.

Influence of the reduction temperature

Table 3 and the associated Figure 3 show the influence of the reduction temperature (300-500°C) on the activity of both Co/P25 and Co/ST01 catalysts, selected as being the more performant Co catalyst supported on an anatase/rutile mixed phase TiO_2 and a very low activity catalyst supported on pure anatase TiO_2, respectively. Regardless of the reduction temperature, the reaction was highly selective and the main reaction product was 2-MTHF. For the Co/P25 catalyst, similar performances were obtained for a reduction temperature of 400°C and 500°C, while lowering the temperature to 300°C resulted to a decrease in both the GVL conversion and the yield to 2-MTHF, to 70% and 56%, respectively.

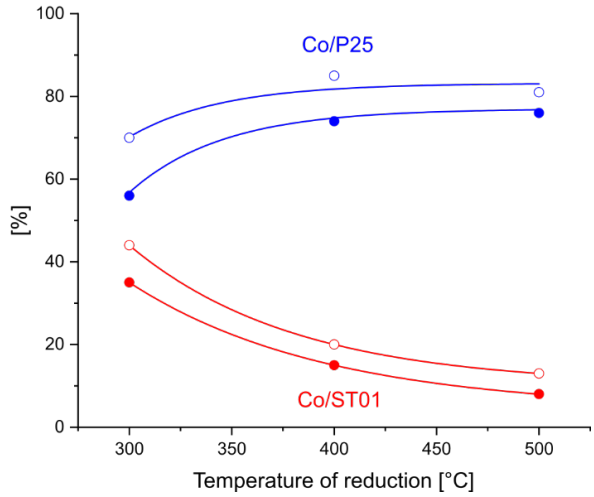

Figure 3. Influence of the reduction temperature on the GVL conversion (○) and the yield to 2-MTHF (●) obtained with Co/P25 and 10%Co/ST01 catalysts, expressed as blue and red symbols, respectively.

This contrasted with the Co/ST01 catalyst. Decreasing the reduction temperature from 500°C to 300°C resulted in a progressive increase in both the GVL conversion and the yield to 2-MTHF, that reached 44% and 35% at 300°C, respectively.

The reduction temperature did not significantly influence the mean size of the Co crystallites on both supports (Table S5), but influenced the nature of the Co phase in the case of both TiO_2 ST01 and P25 supports. Indeed, taking the TiO_2 ST01 support as example, the HRTEM results shown in Figure 2C reveal inter-planes distance and FFT pattern characteristic of the (111) planes of the CoO phase after reduction at 300°C in addition to those of metallic Co. The only partial reduction of the supported Co phases at 300°C correlated well with the reduction profile recorded during the dynamic TPR analysis.

FTIR spectra of CO adsorbed on the Co/TiO_2 catalysts were recorded to characterize the influence of the reduction temperature on the catalyst properties for the two selected supports (Figure 4). The spectra revealed several types of CO adsorption sites dependent on both the temperature reduction and type of support. In agreement with the literature for Co/TiO_2 samples, the spectra were characterized by three spectral regions, with vibration bands in the range of wavenumber from 2100 cm^{-1} to 2000 cm^{-1} assigned to linear CO adsorption on Co crystallites, bands below 2000 cm^{-1} attributed

Catalyst	Reduction temperature [°C]	Product yield [%]						GVL conversion [%] [a]
		2-MTHF	BuOH	2-PeOH	1-PeOH	VA	PDO	
Co/P25	**300**	56	3	5	6	0	0	70
	400	74	1	2	8	0	0	85
	500	76	0	5	0	0	0	81
Co/ST01	**300**	35	0	0	4	1	4	44
	400	15	0	0	1	2	2	20

500	8	0	0	0	3	2	13

Table 3. Influence of the reduction temperature on the catalytic efficiency of the Co/P25 and Co/ST01 catalysts in the GVL hydrogenation in terms of GVL conversion.

Reaction conditions: 230°C; 5h; 0.6 g of1 g GVL; 30 ml 1,4-dioxane and 50 bar H_2
[a] the GVL conversion can be expressed as the sum of the different yields.

to bridged CO adsorption on Co crystallites, and those in the 2200-2150 cm^{-1} range corresponding to CO adsorbed on Ti^{4+} cations[29].

First, independently of the reduction temperature, strongly higher intensity bands were observed for the catalysts supported on the rutile-containing TiO_2 P25 in comparison to the bands with pure anatase (ST01). On the Co/P25-300 sample, the most intense band corresponded to CO linearly adsorbed on $Co^{\delta+}$ with a tail at lower wavenumbers resulting from the linear adsorption of CO on metallic Co[30]. The presence of $Co^{\delta+}$ at the TiO_2 surface might correspond to Co species in interaction with the TiO_2 support, within an interfacial $CoTi_xO_y$ phase or engaged in a Co-O-Ti bond via the high electronegativity surface oxygen atom. Secondary bands at about 1937 cm^{-1} and 1850 cm^{-1} were ascribed to bridge-bonded CO on metallic Co crystallites. Reducing the catalyst at 500°C did not significantly modify the pattern but resulted in a small shift in wavenumbers for both linear and bridged adsorptions, with more clearly pronounced $Co^{\delta+}$ and Co^0 linearly bonded contributions. As no significant differences in terms of mean Co nanoparticle size was observed (at 4 nm), this might be attributed to an increased interaction between the Co phase and the TiO_2 support that can weaken the interaction between the metal and the adsorbed CO molecules, or to the strengthen of the dipole-dipole interaction for adjacent CO molecules, that shifts the absorption

bands towards higher wavenumbers [31,32]. This latter effect may be the result of an increased number of CO adsorption centers on the catalyst surface due to the higher reduction temperature. Only the appearance of a new low wavenumber band at 1870 cm^{-1} was observed, that is usually assigned to CO located in the threefold hollow sites[33,34].

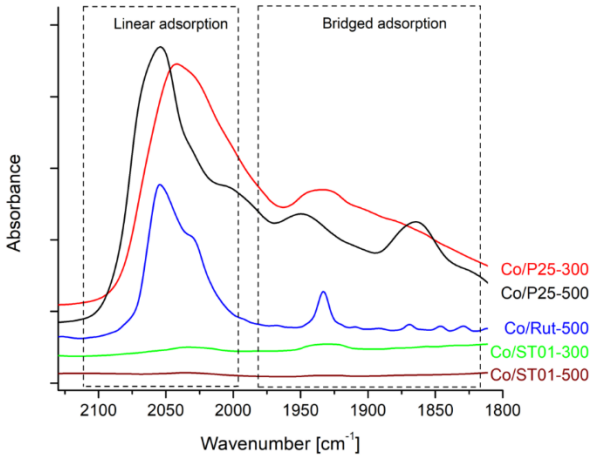

Figure 4. FTIR spectra of CO adsorbed on Co catalysts supported on TiO_2 P25 and TiO_2 ST01 after reduction at 500°C and 300°C. CO-adsorbed FTIR spectrum of the Co/Rut-500 catalyst is also reported.

The much less intense CO vibration bands recorded for the ST01-based catalysts in comparison to the Co/P25 counterparts revealed the limited adsorption of the probe molecule in the case of pure anatase supports, that may be related to a strong metal-support interaction (SMSI effect), reported to be stronger on the anatase polymorph support[35,36]. Indeed, the lowering of the band intensities was not observed for the Co

catalyst based on the pure rutile phase support. With pure anatase TiO_2, the ability of the CO to be chemisorbed in this case is suppressed by TiO_{2-x}, which migrate from the support and decorate the Co nanoparticles.

Catalyst stability and reusability

Reusability experiments were carried out with the most promising catalyst, namely Co/P25 with a reduction temperature of 500°C. A direct reuse of the catalyst without any washing or drying step led to a gradual decrease in the performances, both in terms of GVL conversion and yield to 2-MTHF, that dropped down from 81% and 76%, to 38% and 28%, respectively (Table S6). This could be related to the formation of a carbon deposit[9,37]. For instance, Obregon et al. related the catalyst deactivation with test cycles to the evidence of a poisoning carbon deposit at the catalyst surface, that might be produced from the solvent, as well as from the substrates or the reaction intermediates.

By contrast, submitting the spent catalyst to a drying step at 120°C for 2 h, followed by a calcination at 500°C for 5 h and a final reduction step under H_2 at 500°C for 1 h allowed for the stabilization over five reaction cycles of both the GVL conversion and the yield to 2-MTHF at 81% ± 1% and 72% ± 1%, respectively (Figure 5). This strategy ensured the catalyst stability and achieved stability up to the fifth cycle.

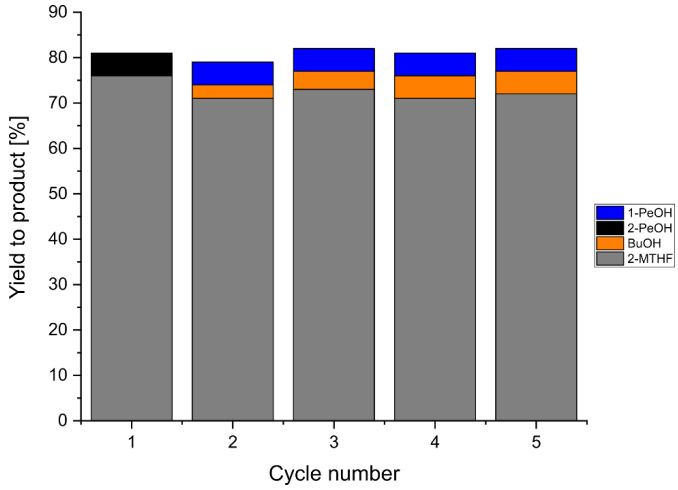

Figure 5. The recycling results for the Co/P25 catalyst, with a proper sequential regeneration protocol consisting in a drying (120°C/2h), a calcination (500°C/5h) and a final reduction under H_2 (500°C/1h). Reaction conditions: 230°C; 5h; 0.6 g of catalyst, 1 g GVL; 30 ml 1,4-dioxane and 50 bar H_2.

Discussion

The activity of TiO_2 supported Co catalysts in the hydrogenation of GVL to 2-MTHF was investigated, and several key factors with significant influence on the reaction have been identified.

Catalyst surface area

Figure 6 evidence the direct relationship existing between the specific surface area of the catalyst and both the yield to 2-MTHF and the GVL conversion. The higher the surface area of the Co/TiO_2 catalyst, the lower the yield to 2-MTHF and the GVL conversion. High surface area catalysts (>85 m^2/g) such as Co/G5, Co/PC500 and

Co/ST01 achieved GVL conversions and yields lower than 10%, while Co/Rut and Co/P90 catalysts with a specific area of about 65 m^2/g achieved intermediate GVL conversions and yields of about 42-56%, and 33-43%, respectively. The highest GVL conversion (81%) and the highest yield to 2-MTHF (76%), with in consequence the highest selectivity to 2-MTHF, was obtained with the catalyst with the smallest specific surface area (49 m^2/g), namely the Co/P25 catalyst. Xaba and de Villiers indicated that the use of high surface area supports can promote the sintering of the supported Co particles[23]. In comparison with the supports containing both anatase and rutile phases, they determined using XRD and TEM analyses that the strongest sintering of Co particles was taking place on the anatase support and was promoted by the high reduction temperature causing the formation of defects on the TiO_2 surface, as well as by the small pore size of the support.

It is known that only supports fully composed of the TiO_2 anatase phase can reach high specific surface areas (PC500, G5, ST01). By contrast commercial supports with mixed anatase/rutile phases display lower surface areas (P25, P90), the surface area decreasing with increasing the rutile content. The phase composition and the surface area of the TiO_2 supports have subsequently direct influence on a variety of parameters that are discussed in the further sub-sections.

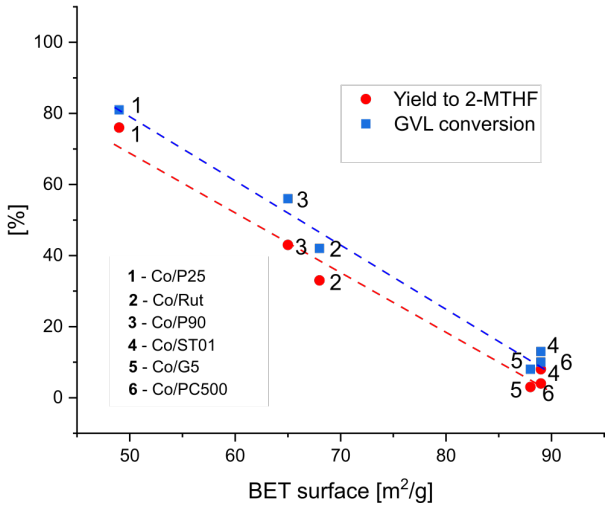

Figure 6. Influence of the specific surface area of the Co/TiO_2 catalyst on the GVL conversion and the yield to 2-MTHF.

Co particle size

Taking into account the influence of the Co crystallite size on the activity of the tested catalysts, the Co crystallite size did not play a significant role in the catalyst performance in the case of supports consisting solely of the TiO_2 anatase phase. This was not the case with the catalysts containing the rutile phase.

Figure 7 shows the effect of the mean Co crystallite size on the catalyst behaviour, whether the support contains rutile TiO_2 partially or entirely. The highest activity was obtained for the Co catalyst deposited on the P25 support, on which the smallest size of Co crystallites (4 nm) was obtained. The small size of the crystallites allowed for a significant improvement in both GVL conversion and the yield to 2-MTHF. It is worth noting that in the case of supports with a low content of rutile phase and pure rutile, the crystallites were larger. It can be concluded that there is an optimum ratio between

the rutile and anatase phases ensuring the achievement of small size of the metal crystallites on the support surface.

In the case of the hydrogenation of levulinic acid to GVL, the ability of the metal particle size to strongly impact the performances of Ru-titania catalysts was reported and evidenced in the case of several TiO_2-based supports[38]. Here, the dependence observed for the cobalt particle size could be related to the difficulty to reach small size particles on anatase, or to their detrimental decoration by titania through SMSI effect, reported to be stronger for the anatase phase vs. the rutile counterpart (see the relevant section).

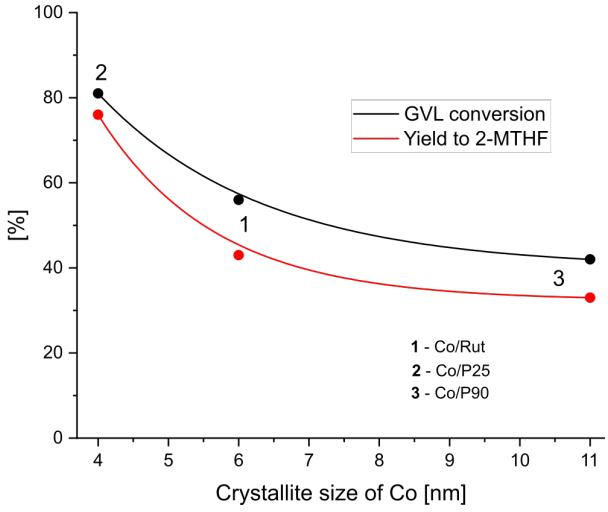

Figure 7. Influence of the Co mean crystallite size on both the GVL conversion and the yield to 2-MTHF for the Co/TiO_2 catalysts (red. 500°C) based on rutile-containing supports.

Catalyst acidity

Although there is no straightforward relationship, the catalyst acidity is suggested to be a factor impacting on the catalyst performances, as illustrated in Figure 8. It shows that possessing

a high surface acidity is necessary requirement for the catalyst, but is not a sufficient condition. Indeed, the Co/P25 catalyst with the highest surface acidity of 6.5 µmol/m^2 reached the highest performances. By contrast, Co/Rut, Co/PC500 and Co/G5 catalysts with an intermediate surface acidity of 3.7-4.1 µmol/m^2 differed strongly in terms of performances, with a moderate 2-MTHF yield (and GVL conversion) for the Co/Rut catalyst, while conversions and yields lower than 10% were obtained for the both Co/PC500 and Co/G5 catalysts.

According to the literature, the rate of GVL hydrogenation can be determined by the acid sites[27]. Obregon et al.[9] indicated that one of the limiting factors of the hydrogenation of GVL to 2-MTHF was the too low acidity of Ni-Cu catalysts. Indeed, acid sites are known to catalyse the dehydration of the 1,4-PDO intermediate to 2-MTFH, while however the most difficult, rate determining, reaction step is the initial ring-opening hydrogenation that forms 1,4-PDO[6]. In our case, the very low yields to 1,4-PDO observed (within the 0-3% range whatever the activity of the catalyst) suggested that 1,4-PDO is directly and rapidly converted to 2-MTHF[39] what might explain the absence of any clear relationship between the catalytic efficiency and the acidity.

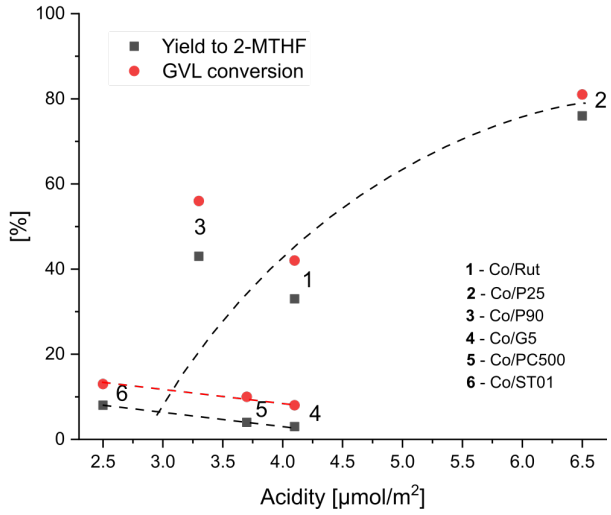

Figure 8. Influence of the acidity of the Co/TiO_2 catalyst (red. 500ºC) on the GVL conversion and the yield to 2-MTHF.

Metal-support interaction and TiO_2 crystalline structure

An important factor influencing the activity of the catalysts was the interaction of the TiO_2 support with the Co particles. The results demonstrate that the presence of the rutile phase within the TiO_2 support is strongly beneficial to the performances of the Co catalysts, as directly illustrated in Figure 9 for both the GVL conversion and the yield to 2-MTHF. Even the small content of rutile phase of 10-20% in the catalysts supported on P25 and P90 strongly improved the GVL conversion and the yield to 2-MTHF in comparison to those obtained with the catalysts supported on pure anatase.

However, it must be noted that the co-presence of the anatase phase was also strongly beneficial, as the catalyst supported on pure rutile TiO_2 showed only moderate GVL conversion and 2-MTHF yield. This evidenced the existence of an optimum in terms of rutile and anatase phase ratio. It is worth noting that the presence of the rutile phase

causes the catalyst reduction temperature shift towards a higher temperature. It is related to the strong interaction of Co with the support. However, it should be emphasized that, according to the literature data, increasing the degree of interaction of Co with the support increases the dispersion of the metal[40]. The beneficial input of the rutile polymorph on the activity of Co catalysts was highlighted by Shimura et al.[41] in the Fischer-Tropsch (FT) synthesis and by Jongsomjit et al. [42] in the CO hydrogenation.

The catalysts based on pure anatase supports are subjected to the much stronger SMSI effect exhibited by the anatase phase during the reduction process in comparison to its rutile counterpart[35,36,43] as a result of a higher mobility of titanium. In consequence, although reducing the catalyst at the high temperature of 500°C formed metallic cobalt regardless of the support nature (pure anatase or mixed anatase-rutile phases, the presence of a SMSI effect leads to a different availability of the metallic cobalt active sites depending on the nature of the interfaced titania support. Indeed, in the case of pure anatase supports, the increase in the reduction temperature necessary to get full reduction of the Co nanoparticles is accompanied by a lower availability of the Co^0 surface sites to the reactants. By contrast, in the case of an anatase-rutile mixed phase support, FTIR results suggested the preferential location of the Co nanoparticles at the surface of the rutile phase. Similar hypothesis was drawn in our earlier works in the case of TiO_2 supported Ru catalysts,[12,13] as well as by Kim et al. [26] Moreover, Huber et al.[36] observed that in the case of the P25 support, despite the decoration of the Co particles by TiO_2, metallic cobalt is still available. This allowed the

metallic cobalt active sites to maintain a high degree of availability after reduction at high temperature.

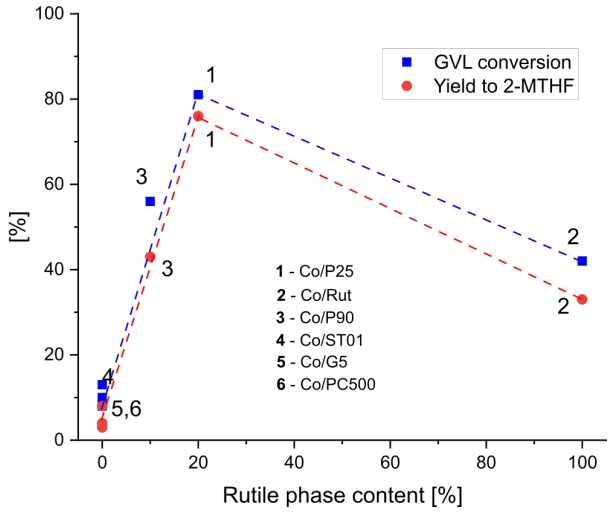

Figure 9. Influence of the rutile phase content of the TiO_2 support on the GVL conversion and the yield to 2-MTHF.

Conclusions

In this work, we discussed the key-parameters allowing to reach a high yield to 2-MTHF on robust and stable Co/TiO_2 catalysts. First, the crucial role of the titania support as a tool enabling to control the degree of availability of metallic Co nanoparticles and the activity of the catalysts was highlighted. We showed that the co-presence of both rutile and anatase phases in the TiO_2 support was strongly beneficial for reaching high yields to 2-MTHF. The surface acidity was shown to be a requested property for the catalyst, but was not a sufficient factor allowing to reach high activity.

On one hand, the Co interaction with the rutile phase was shown to be stronger than for the anatase counterpart, what influenced the dispersion of the metal. The size of Co particles plays an important role for rutile-containing catalysts. By contrast, it is not a key-parameter for the anatase TiO_2 supports, and we proposed that the low performances of Co catalysts supported on pure anatase resulted from the decoration of Co nanoparticles by TiO_2 through SMSI effect, what consequently reduces the surface availability of Co nanoparticles. However, their availability on pure anatase TiO_2 support can be tuned by the reduction temperature.

Conflicts of interest

There are no conflicts to declare.

Acknowledgements

The authors acknowledge gratefully the National Center of Science (NCN), Krakow, Poland, for financially supporting the work through a SONATA BIS grant (2016/22/E/ST4/00550).

Notes and references

1 R. Narayan, in *Biomass for Renewable Energy, Fuels, and Chemicals*, 1992, pp. 1–10.

2 J. F. Leal Silva, A. P. Mariano and R. Maciel Filho, *Biomass and Bioenergy*, 2018, **119**, 492–502.

3 A. T. Adeleye, H. Louis, O. U. Akakuru, I. Joseph, O. C. Enudi and D. P. Michael, *AIMS Energy*, 2019, **7**, 165–185.

4 Y. Shao, S. Ba, K. Sun, G. Gao, M. Fan, J. Wang, H. Fan, L. Zhang and X. Hu, *Chem. Eng.*

J., 2022, **429**, 132433.

5 J. C. Serrano-Ruiz, R. M. West and J. A. Dumesic, *Annu. Rev. Chem. Biomol. Eng.*, 2010, **1**, 79–100.

6 M. G. Al-Shaal, A. Dzierbinski and R. Palkovits, *Green Chem.*, 2014, **16**, 1358–1364.

7 D. Licursi, C. Antonetti, S. Fulignati, M. Giannoni and A. M. Raspolli Galletti, *Catalysts*, 2018, **8**, 277.

8 D. Sun, T. Saito, S. Otsuka, T. Ozawa, Y. Yamada and S. Sato, *Appl. Catal. A Gen.*, 2020, **590**, 117309.

9 I. Obregón, I. Gandarias, A. Ocio, I. García-García, N. Alvarez de Eulate and P. L. Arias, *Appl. Catal. B Environ.*, 2017, **210**, 328–341.

10 Q. Liu, Z. Zhao, M. Arai, C. Zhang, K. Liu, R. Shi, P. Wu, Z. Wang, W. Lin, H. Cheng and F. Zhao, *Catal. Sci. Technol.*, 2020, **10**, 4412–4423.

11 G. Novodárszki, H. E. Solt, J. Valyon, F. Lónyi, J. Hancsók, D. Deka, R. Tuba and M. R. Mihályi, *Catal. Sci. Technol.*, 2019, **9**, 2291–2304.

12 A. M. Ruppert, J. Grams, M. Jędrzejczyk, J. Matras-Michalska, N. Keller, K. Ostojska and P. Sautet, *ChemSusChem*, 2015, **8**, 1538–1547.

13 M. Brzezinska, J. Niemeier, Y. Louven, N. Keller, R. Palkovits and A. M. Ruppert, *Catal. Sci. Technol.*, 2020, **10**, 6860–6869.

14 B. Tapin, F. Epron, C. Especel, B. K. Ly, C. Pinel and M. Besson, *ACS Catal.*, 2013, **3**, 2327–2335.

15 M. Przydacz, M. Jędrzejczyk, M. Brzezińska, J. Rogowski, N. Keller and A. M. Ruppert, *J. Supercrit. Fluids*, 2020, **163**, 104827.

16 P. Scardi, L. B. Mccusker, R. B. Von Dreele, D. E. Cox and D. Loue, *J. Appl. Crystallogr.*,

1999, **32**, 36–50.

17 J. Rodriguez-Carvajal, *Phys. B*, 1993, **192**, 55–69.

18 A. Ocio, P. L. Arias, I. Obregón, I. Gandarias and N. Miletic, *ChemSusChem*, 2015, **8**, 3483–3488.

19 P. Cai, S. Ci, E. Zhang, P. Shao, C. Cao and Z. Wen, *Electrochim. Acta*, 2016, **220**, 354–362.

20 B. Jongsomjit, C. Sakdamnuson, J. G. Goodwin and P. Praserthdam, *Catal. Letters*, 2004, **94**, 209–215.

21 B. A. Sexton, A. E. Hughes and T. W. Turney, *J. Catal.*, 1986, **97**, 390–406.

22 K. Takanabe, K. Nagaoka, K. Nariai and K. I. Aika, *J. Catal.*, 2005, **230**, 75–85.

23 B. M. Xaba and J. P. R. De Villiers, *Ind. Eng. Chem. Res.*, 2016, **55**, 9397–9407.

24 F. Liu, J. Ftouni, P. C. A. Bruijnincx and B. M. Weckhuysen, *ChemCatChem*, 2019, **11**, 1–11.

25 T. Omotoso, S. Boonyasuwat and S. P. Crossley, *Green Chem.*, 2014, **16**, 645–652.

26 A. A. Kim, D. P. Debecker, A. Kim, D. P. Debecker, F. Devred, V. Dubois, C. Sanchez and S. Capucine, *Appl. Catal. B, Environ.*, 2018, **220**, 615–625.

27 Y. B. Huang, A. F. Liu, Q. Zhang, K. M. Li, W. B. Porterfield, L. C. Li and F. Wang, *ACS Sustain. Chem. Eng.*, 2020, **8**, 11477–11490.

28 G. Novodárszki, H. E. Solt, G. Lendvay, R. M. Mihályi, A. Vikár, F. Lónyi, J. Hancsók and J. Valyon, *Catal. Today*, 2019, **336**, 50–62.

29 C. Deiana, E. Fois, G. Martra, S. Narbey, F. Pellegrino and G. Tabacchi, *ChemPhysChem*, 2016, **17**, 1956–1960.

30 J. Li and N. J. Coville, *Appl. Catal. A Gen.*, 1999, **181**, 201–208.

31 G. Blyholder, *J. Phys. Chem.*, 1964, **68**, 2772–2778.

32 M. Scheffler, *Surf. Sci.*, 1979, **81**, 562–570.

33 C. J. Weststrate, J. Van De Loosdrecht and J. W. Niemantsverdriet, *J. Catal.*, 2016, **342**, 1–16.

34 A. Frederic, C. Meunier, A. Paredes-nunez, L. Burel, D. Motta-meira, N. Guilhaume and Y. Schuurman, *Angew. Chemie*, 2017, **130**, 556–559.

35 F. Bertella, P. Concepción and A. Martínez, *Catal. Today*, 2017, **289**, 181–191.

36 J. Lee, S. P. Burt, C. A. Carrero, A. C. Alba-Rubio, I. Ro, B. J. O'Neill, H. J. Kim, D. H. K. Jackson, T. F. Kuech, I. Hermans, J. A. Dumesic and G. W. Huber, *J. Catal.*, 2015, **330**, 19–27.

37 S. K. Bhargava, J. Tardio and K. Reddy, *RSC Adv.*, 2016, **6**, 9872–9879.

38 J. Wojciechowska and M. Je, *ChemSusChem*, 2019, 1–13.

39 J.J. Bozell, L. Moens, D.C. Elliott, Y. Wang, G.G. Neuenscwander, S. W. Fitzpatrick, R.J. Bilski and J.L. Jarnefeld, *Resour. Conserv. Recycl.*, 2000, **28**, 227–239.

40 K. Suriye, P. Praserthdam and B. Jongsomjit, *Ind. Eng. Chem. Res.*, 2005, **44**, 6599–6604.

41 K. Shimura, T. Miyazawa, T. Hanaoka and S. Hirata, *Appl. Catal. A Gen.*, 2013, **460**–**461**, 8–14.

42 B. Jongsomjit, T. Wongsalee and P. Praserthdam, *Catal. Commun.*, 2005, **6**, 705–710.

43 V. A. De La Peña O'Shea, M. Consuelo Álvarez Galván, A. E. Platero Prats, J. M. Campos-Martin and J. L. G. Fierro, *Chem. Commun.*, 2011, **47**, 7131–7133.

TiO_2 supported Co catalysts for the hydrogenation of γ-valerolactone to 2-methyltetrahydrofuran: influence of the support

Emilia Soszka[1], Marcin Jędrzejczyk[1], Christophe Lefèvre[3], Dris Ihiawakrim[3], Nicolas Keller[2], Agnieszka M. Ruppert[1*]

[1] Institute of General and Ecological Chemistry, Lodz University of Technology, ul. Żeromskiego 116, 90-924 Łódź, Poland

[2] Institut de Chimie et Procédés pour l'Energie, l'Environnement et la Santé (ICPEES), CNRS/University of Strasbourg, 67087 Strasbourg, France ; nkeller@unistra.fr

[3] Institut de Physique et Chimie des Matériaux de Strasbourg (IPCMS), CNRS/University of Strasbourg, 67034 Strasbourg, France

*Corresponding author: agnieszka.ruppert@p.lodz.pl

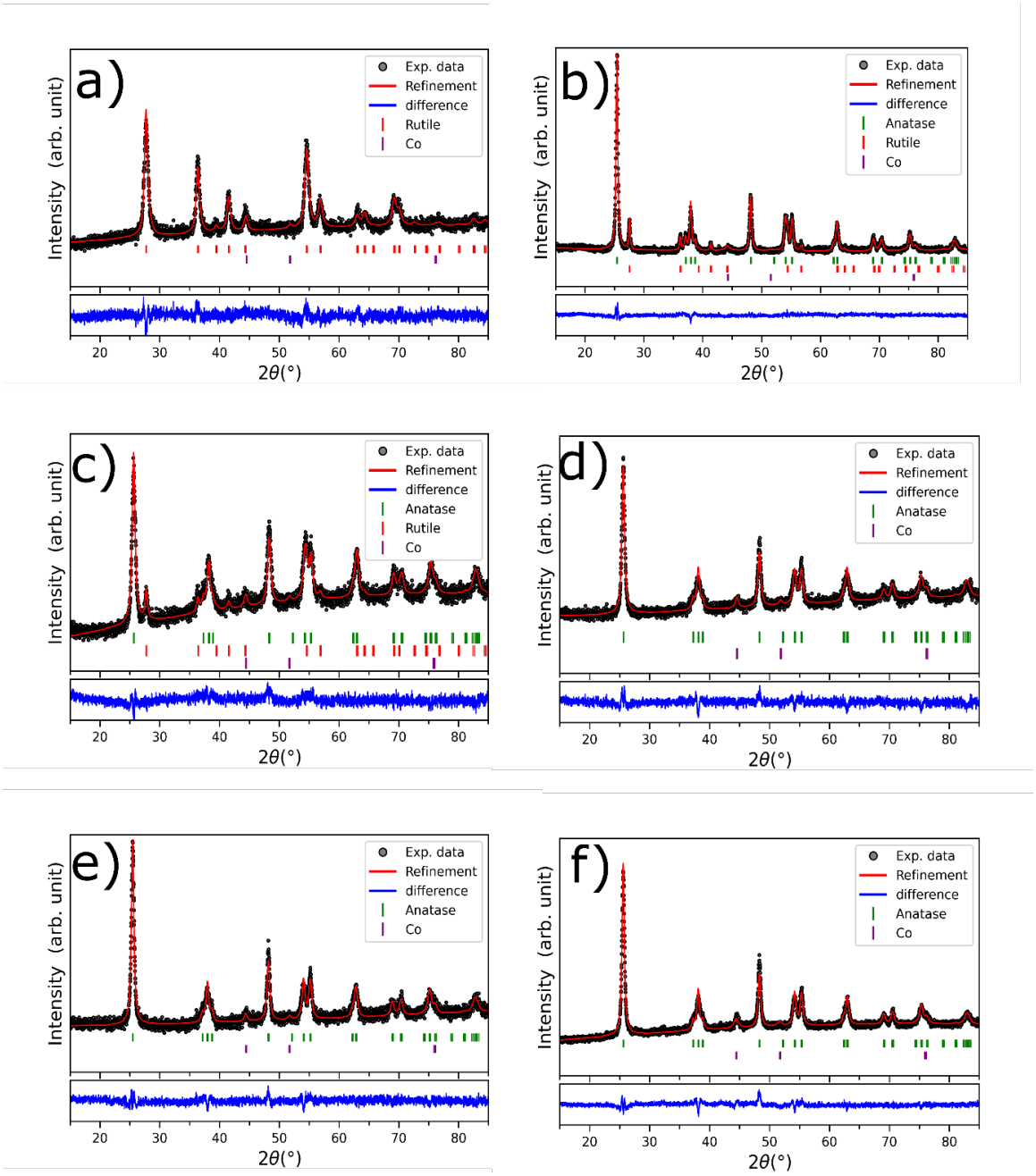

Figure S1. Powder XRD patterns of the 10% Co/TiO_2 catalysts after reduction at 500°C, a) 10%Co/R, b) 10%Co/P25, c) 10%Co/P90, d) 10%Co/G5, e) 10%Co/PC500, f) 10%Co/ST01. The positions of the Bragg reflections are represented by vertical bars, in green for the reflexes indexed in the I41/amd tetragonal unit cell of anatase TiO_2, in red for those of the P42/mnm tetragonal unit cell of rutile TiO_2, and in purple for those of the Fm-3m cubic unit cell of metallic Co phase.

Table S1. Crystallographic cell parameters of TiO_2 and Co phases obtained after Rietveld refinement.

Catalysts	Anatase (I41/amd)		Rutile (P42/mnm)		Cobalt (Fm-3m)
	a (Å)	c (Å)	a (Å)	c (Å)	a (Å)
Rut			4.602(2)	2.962(2)	3.550(5)
P25	3.787(1)	9.507(1)	4.598(1)	2.959(1)	3.549(7)
P90	3.796(1)	9.514(2)	4.608(2)	2.965(3)	3.554(9)
G5	3.794(1)	9.519(2)			3.545(5)
PC500	3.793(1)	9.524(2)			3.549(4)
ST01	3.791(1)	9.519(2)			3.554(-)

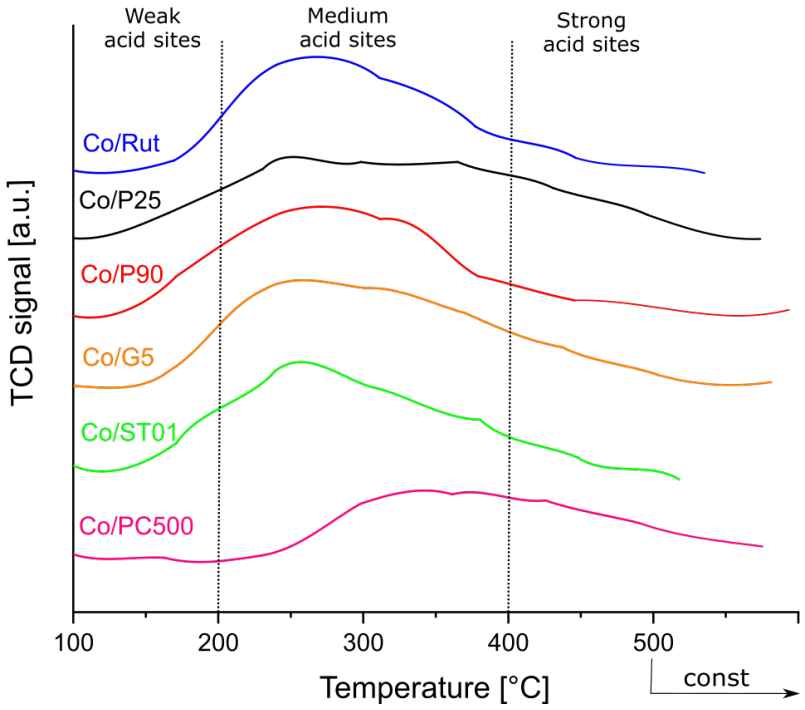

Figure S2. NH_3-TPD curves recorded for the different Co/TiO_2 catalysts.

The surface acidity of the different Co/TiO_2 catalysts was evaluated through the temperature-programmed desorption of ammonia (NH_3-TPD), the temperature of ammonia desorption indicating the strength of the acid centers at the catalyst surface. Ammonia desorbs from weak centers below the temperature of 200°C, in the 200-400°C range for medium-strength centers, while peaks above 400°C are assigned to strong acid centers on the catalyst surface[2,3].

Medium strength acid centers dominate on the surface of all catalysts. In addition, both catalysts based on PC500 and P25 expose as well significant amounts of stronger acidic centers, while all catalyst except the one based on PC500 contain also a rather similar contribution of weak acid centers. Due to the NH_3-TPD profiles recorded with clear overlap between the different strength contributions, it is however difficult to assess quantitively the number of the acidic sites depending on their strength, and therefore the overall acidity of the catalysts has been reported in Table 1 in the manuscript

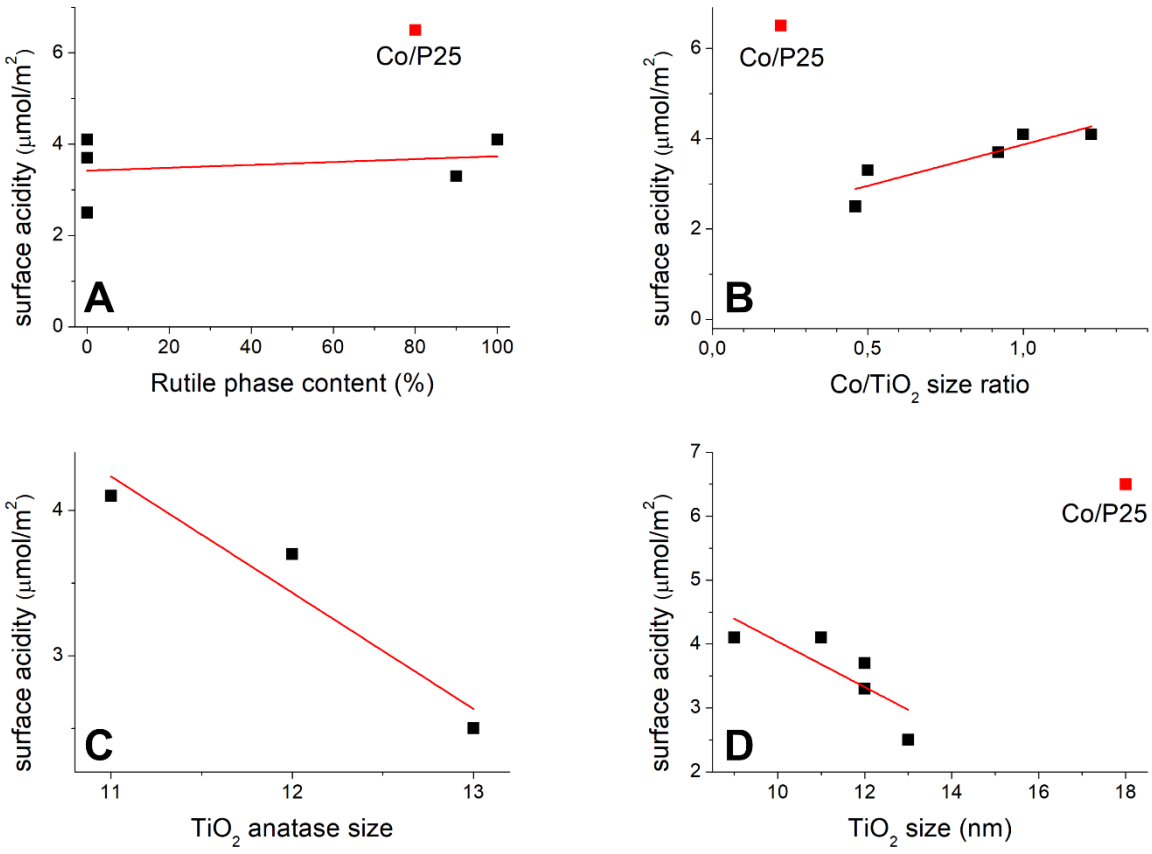

Figure S3. Influence of some selected parameters on the surface acidity of Co/TiO_2 catalysts expressed in µmol/m^2. **(A)** Rutile phase content, **(B)** Co/TiO_2 size ratio, **(C)** TiO_2 anatase size for pure anatase-containing catalysts, **(D)** TiO_2 size ratio for all catalysts.

Table S2. Hydrogen uptake of Co/TiO_2 catalysts during H_2-TPR analysis.

Catalyst	Hydrogen uptake [µmol*g^{-1} cat][a]
Co/Rut	2180 ± 200
Co/P25	2061 ± 206
Co/P90	2132 ± 210
Co/G5	2391 ± 210
Co/PC500	2185 ± 215
Co/ST01	2251 ± 220

[a] Calculated from the integration of the H_2-TPR curve

The H_2-TPR measurements were performed as usual in the dynamic mode, with a fast temperature ramp of 25°C/min. Such a dynamic mode with fast heating rate is known to slightly push towards higher temperatures, the temperature of complete reduction for all samples, in comparison to the static mode usually used for the catalyst reduction (here with a final temperature maintained for 1 h). Therefore, the H_2-TPR profile was integrated till 550°C or 650°C depending on the catalysts.

The accuracy of measurements has been estimated to ca.10% by triplicating TPR experiments on different samples. This finds its origin notably in the different water contents of the samples due to the presence of surface hydroxyl groups that condense/dehydrate during the analysis (the H_2 uptake being normalized per g of catalyst), in the uncertainty in the TCD baseline used for the calculation, and in the occurrence of spillover of hydrogen from the Co particles to the metal–support interface[1]. Taking that into account, the calculated uptakes of hydrogen correspond to a complete reduction of the supported cobalt oxide nanoparticles for all Co/TiO_2 catalysts reduced at 500°C, as the complete reduction of the cobalt species should correspond to a theoretical H_2 uptake of 2270 µmol*g^{-1}_{cat}, based on the equation $Co_3O_4 + 4H_2 \rightarrow 3Co + 4H_2O$.

As mentioned above, it is worth noting that during the reduction process not only cobalt oxide is reduced, but also the surface TiO_2 might become partially reduced via spillover of hydrogen from the cobalt particles to the metal–support interface. However, this contribution is negligible in comparison to the values of hydrogen uptake reached for the reduction of cobalt oxide species. As it may concern only the external surface of the TiO_2 support crystallites, the reduction degree of the TiO_2 support is therefore negligible.

Table S3. GVL elimination and sum of the product yields obtained when submitting the TiO_2 support alone to the reaction conditions in the presence of the GVL substrate.

Titania support	GVL elimination [%]	Sum of the product yields [%]
-	4	0
P90	30	0
ST01	39	0
P25	33	0
P25 after reduction at 500°C	28	0

Reaction conditions: GVL, 0.6 g of titania support, 230°C; 5 h; 30 ml 1,4-dioxane and 50 bar H_2

Table S4. Effect of the extension of the reaction time from 5 h to 6 h on the catalytic efficiency of the Co/P90 catalysts in the GVL hydrogenation process in terms of yields to the different products, GVL elimination, GVL conversion and carbon imbalance.

Time of reaction [h]	Product yield [%]						GVL elimination [%]	GVL conversion [%] [a]	Carbon imbalance [%] [b]
	2-MTHF	BuOH	2-PeOH	1-PeOH	VA	PDO			
5	43	4	1	5	0	3	89	56	33
6	63	2	3	7	0	0	91	75	16

Reaction conditions: 230°C; 0.6 g of catalyst, 1 g GVL; 30 ml 1,4-dioxane and 50 bar H_2

[a] the GVL conversion expressed as the sum of the different yields

[b] calculated as the difference between the GVL elimination and the sum of the different yields

Table S5. Influence of the reduction temperature on the mean size of Co crystallites in the Co/P25 and Co/ST01 catalysts.

Catalyst	Reduction temperature [°C]	Crystallite size [nm]
Co/P25	300	4(1)
Co/ST01	300	5(1)
Co/P25	500	4(1)
Co/ST01	500	6(1)

Table S6. The recycling results for the 10%Co/P25-500 catalyst without any treatment of the spent catalyst between consecutive cycles.

Cycle of reaction	Product yield [%]						GVL conversion [%] [a]
	2-MTHF	BuOH	2-PeOH	1-PeOH	VA	PDO	
1	76	0	5	0	0	0	81
2	63	0	0	4	0	5	72
3	27	0	0	2	0	15	44
4	28	0	0	2	0	8	38

Reaction conditions: 230°C; 5h; 0.6 g of catalyst, 1 g GVL; 30 ml 1,4-dioxane and 50 bar H_2

[a] the GVL conversion expressed as the sum of the different yields

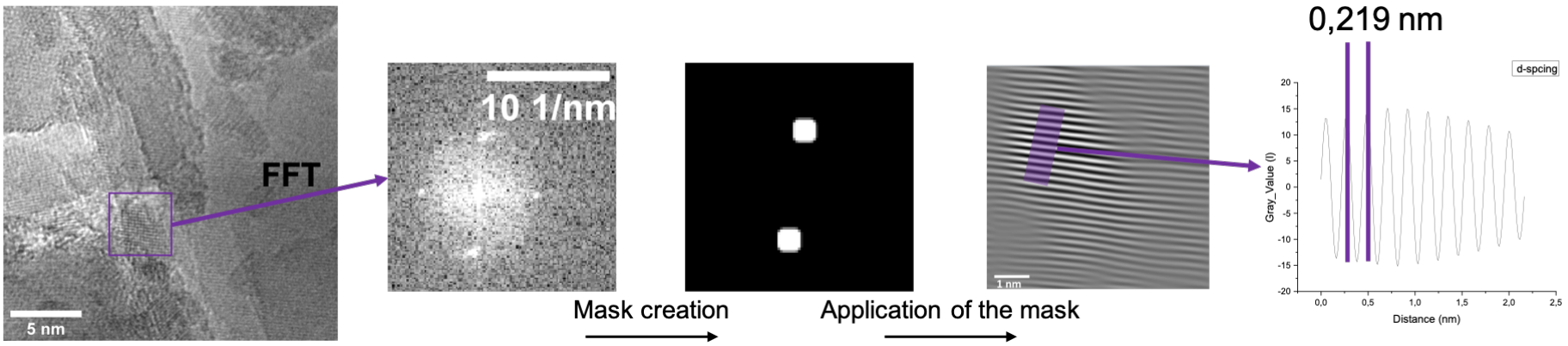

Figure S4. Principle of the measurement of d-spacings. Each image was processed using Digital Micrograph (Gatan). We first computed an autocorrelation image of a selected area of the HRTEM image to reinforce information about periodicity in the HRTEM image. The FFT was then calculated from the autocorrelation image. The bright spots observed on the FFT (which represent periodicities) were subsequently selected using a mask, before we ran the inverse FFT (IFFT) based only on those spots. The filtered image obtained is highlighting only the periodic information. This final image should be understood as a graphical representation of the periodic nanoparticle inside the selected initial HRTEM image, but not as a TEM image where only the non-periodic features have been removed. The inter plane distances were derived from this graph.

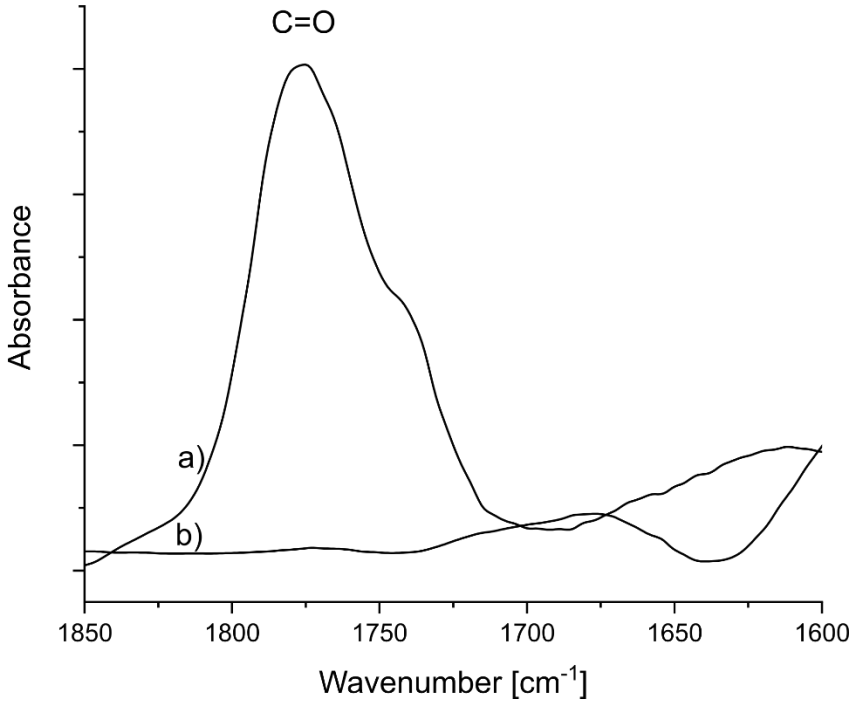

Figure S5. FTIR spectra recorded on the TiO_2 P25 support submitted to the reaction conditions for 5h (a) in the presence and (b) absence of the GVL substrate.

1 V. A. De La Peña O'Shea, M. Consuelo Álvarez Galván, A. E. Platero Prats, J. M. Campos-Martin and J. L. G. Fierro, *Chem. Commun.*, 2011, **47**, 7131–7133.

2 P. Kumar, V. C. Srivastava and I. M. Mishra, *Energy and Fuels*, 2015, **29**, 2664–2675.

3 M. Kurian, S. Thankachan, D. S. Nair, A. E. K, A. Babu, A. Thomas and B. Krishna K. T, *J. Adv. Ceram.*, 2015, **4**, 199–205.